

A Self-Organized ECM-Mimetic Model Based on an Amphiphilic Multiblock Silk-Elastin-Like co-Recombinamer with a Concomitant Dual Physical Gelation Process

Alicia Fernández-Colino, F. Javier Arias, Matilde Alonso, and José Carlos Rodríguez-Cabello

Biomacromolecules, Just Accepted Manuscript • Publication Date (Web): 17 Sep 2014

Downloaded from <http://pubs.acs.org> on September 18, 2014

Just Accepted

“Just Accepted” manuscripts have been peer-reviewed and accepted for publication. They are posted online prior to technical editing, formatting for publication and author proofing. The American Chemical Society provides “Just Accepted” as a free service to the research community to expedite the dissemination of scientific material as soon as possible after acceptance. “Just Accepted” manuscripts appear in full in PDF format accompanied by an HTML abstract. “Just Accepted” manuscripts have been fully peer reviewed, but should not be considered the official version of record. They are accessible to all readers and citable by the Digital Object Identifier (DOI®). “Just Accepted” is an optional service offered to authors. Therefore, the “Just Accepted” Web site may not include all articles that will be published in the journal. After a manuscript is technically edited and formatted, it will be removed from the “Just Accepted” Web site and published as an ASAP article. Note that technical editing may introduce minor changes to the manuscript text and/or graphics which could affect content, and all legal disclaimers and ethical guidelines that apply to the journal pertain. ACS cannot be held responsible for errors or consequences arising from the use of information contained in these “Just Accepted” manuscripts.



A Self-Organized ECM-Mimetic Model Based on an Amphiphilic Multiblock Silk-Elastin-Like co-Recombinamer with a Concomitant Dual Physical Gelation Process

*Alicia Fernández-Colino, F. Javier Arias, Matilde Alonso, J. Carlos Rodríguez-Cabello**

G.I.R. Bioforge, University of Valladolid, CIBER-BBN, Paseo de Belén 11, 47011 Valladolid, Spain

ABSTRACT. Although significant progress has been made in the area of injectable hydrogels for biomedical applications and model cell niches, further improvements are still needed, especially in terms of mechanical performance, stability and biomimicry of the native fibrillar architecture found in the extracellular matrix (ECM). This work focuses on the design and production of a silk-elastin-based injectable multiblock co-recombinamer that spontaneously forms a stable physical nanofibrillar hydrogel under physiological conditions. That differs from previously reported silk-elastin-like polymers on a major content and predominance of the elastin-like part, as well as a more complex structure and behavior of such part of the molecule, which is aimed to obtain well defined hydrogels. Rheological and DSC experiments showed that this system displays a coordinated and concomitant dual gelation mechanism. In a first stage, a rapid, thermally driven gelation of the co-recombinamer solution takes place once the system reaches body temperature due to the thermal responsiveness of the elastin-like (EL) parts and the amphiphilic multiblock design of the co-recombinamer. A bridged micellar

1 structure is the dominant microscopic feature of this stage, as demonstrated by AFM and TEM.
2
3 Completion of the initial stage triggers the second, which comprises a stabilization, reinforcement, and
4
5 microstructuring of the gel. FTIR analysis shows that these events involve the formation of β -sheets
6
7 around the silk motifs. The emergence of such β -sheet structures leads to the spontaneous self-
8
9 organization of the gel into the final fibrous structure. Despite the absence of biological cues, here we
10
11 set the basis of the minimal structure that is able to display such a set of physical properties and undergo
12
13 microscopic transformation from a solution to a fibrous hydrogel. The results point to the potential of
14
15 this system as a basis for the development of injectable fibrillar biomaterial platforms towards a fully
16
17 functional, biomimetic, artificial extracellular matrix and cell niches.
18
19
20
21
22

23 **KEYWORDS.** Elastin-like recombinamers, SELR, hydrogel, fibrillar, artificial extracellular matrix .
24
25
26
27
28
29

30 **INTRODUCTION**

31
32

33 The latest trends in materials science involve the strategy of copying the designs found in Nature in the
34
35 laboratory ¹, since they exhibit extraordinary properties that have been achieved over millions of years
36
37 of evolution. Within this framework, the greatest biomaterials-related challenge in the field of tissue
38
39 engineering is to create biomimetic scaffolds that can act in a similar manner to the extracellular matrix
40
41 (ECM). Given the complexity of the natural ECM, this is a particularly challenging task as the artificial
42
43 ECM (aECM) must reproduce the complex cell-ECM interaction, which includes specific cell adhesion,
44
45 protease sensitivity, and cytokine release, amongst others. In addition, cell-material interactions and the
46
47 group of factors that govern cell fate in the natural ECM are not restricted exclusively to biological
48
49 features, since physical clues are also of relevance. From a structural perspective, the ECM has a
50
51 fibrillar and viscoelastic character, and such biophysical features have been reported to have a
52
53 significant influence on cell behavior ²⁻⁴. Although the molecular pathways involved in cellular
54
55
56
57
58
59
60

1 mechanosensitivity are still open to investigation, it is well known that cells sense and respond to the
2 stiffness of their environment by converting mechanical inputs into chemical outputs ^{5,6}. More recently,
3 cell fate related to energy dissipation mediated by enzymatic ECM degradation has also been reported ⁷.
4
5 Such discoveries highlight the importance of controlling both the more obvious biological environment
6
7 of a bioengineered matrix and the physical one.
8
9

10
11
12
13 One more condition must be added to all those mentioned above, namely that candidate aECMs will
14 eventually be implanted, therefore, in addition to being sufficiently functional, they must satisfactorily
15 cope with the immune rejection system and not be identified as a foreign body. Furthermore, they
16 should be reabsorbed without any damage or stress for growing cells. In light of the above, the creation
17
18 of such aECMs seems to be a major challenge, and more so if we consider that all this must be achieved
19
20 in an injectable formula, in other words a system in a liquid state from which, after implantation
21
22 (injection), all other structures and functions develop; self-organization is a must in this context.
23
24
25
26
27
28
29

30
31 One interesting group of self-assembling polymers is the elastin-like polymers, and particularly their
32 recombinant versions, the elastin-like recombinamers (ELRs) ⁸. ELRs are protein-based materials whose
33 composition is inspired by the primary sequence found in natural elastin. Thus, the amino-acid sequence
34
35 of ELRs is commonly constituted by repeats of the (VPGXG) pentapeptide, where X is any amino acid
36
37 except proline. ELRs show a reversible LCST (Lower Critical Solution Temperature) phase transition,
38
39 usually known as the inverse temperature transition (ITT) in the context of elastin-like materials, in
40
41 response to temperature. In an aqueous medium, below a characteristic temperature known as the
42
43 transition temperature (Tt), the polymer chain remains soluble. However, above this Tt, the ELR
44
45 assembles hydrophobically and adopts a regular, dynamic, nonrandom structure characterized by the
46
47 presence of type II β turns ^{9,10}. Such stimuli-responsive behavior, together with their proven
48
49 biocompatibility ¹¹ and their mechanical performance, have positioned these recombinant
50
51
52
53
54
55
56
57
58
59
60

1 macromolecules as potential candidates for use in numerous biomedical applications ^{12,13}, particularly
2 regarding the development of injectable hydrogels, which mainly relies on their ability to respond to
3 thermal stimulation. As a result of this property, the recombinamer solution can be injected as a liquid
4 but, once inside the organism, it reaches body temperature and consequently undergoes a phase
5 transition from solution to gel that can be referred to as thermo-gelling. In general, homo-ELRs tend to
6 segregate from solution, thus giving rise to a coacervate. However, for a more effective hydrogel
7 formation, ELRs have been designed as multi-block amphiphilic molecules ¹⁴. Thus, the hydrophilic
8 blocks, which do not show LCST behavior under the conditions used, are responsible for water
9 retention, whereas the cross-linking function is achieved by the thermally driven folding and
10 hydrophobic interaction of the hydrophobic blocks. Following this idea, a thermally controlled
11 amphiphilic ELR tetrablock co-recombinamer in which the hydrophobic blocks, which contain
12 isoleucine as guest residue, are responsible for the physical cross-linking by means of a bridged micelle
13 structure at a microscopic level, has been reported previously ¹⁴. Glutamic acid is the guest residue in
14 the remaining two hydrophilic blocks. However, these hydrogels does not show a fibrillar structure upon
15 setting. Additionally, they lose their integrity in contact with an excess of aqueous medium. Under those
16 conditions, the gel swells and, finally, at a molecular level, the material goes from a crosslinked
17 hydrogel to a micellar dispersion. The weak character of noncovalent interactions is the problem
18 common to most physical crosslinking approaches ¹⁵⁻¹⁸.

19
20
21
22
23
24
25
26
27
28
29
30
31
32
33
34
35
36
37
38
39
40
41
42
43
44 With regard to the fibrillar architecture, polymer processing technologies such as electrospinning have
45 been applied to obtain fibers on the nanometric scale ¹⁹. However, the main handicap of this approach is
46 to place cells within a nanofibrillar structure with pore sizes smaller than cellular diameters. As a result,
47 strategies that allow nanofibrillar networks to be formed *in situ* are preferred. An excellent approach for
48 obtaining nanofibers takes advantage of molecular self-assembly ^{20 21}. In this regard, researchers have
49 fixed their attention on self-assembled motifs present in Nature, such as coiled-coiled structures, β -sheet
50
51
52
53
54
55
56
57
58
59
60

1 structures, or β -hairpins and have incorporated such designs, sometimes with suitable modifications, to
2 obtain nanostructures with a well-defined shape.
3
4

5
6 In this context, SL motifs have been reported to spontaneously adopt a β -sheet structure, which is
7 characterized by its stability^{22,23}. The stable nature of the β -sheet conformation adopted, together with
8 their biocompatible nature, has propelled the development of a wide range of silk-inspired materials^{24,25}
9 and silk-elastin inspired materials. SELRs have already proven to display a synergic effect in which the
10 elastin-like (EL) part, which tends to have a relatively simple composition in the examples found in the
11 literature, reduces the degree of crystallinity of the SL blocks while enhancing the elastic properties of
12 the combination²⁶. However, the stimuli-responsiveness of the EL block has not been exploited to any
13 great extent to date and no complex molecular designs for that block showing advanced functionality
14 have been reported. Furthermore, many SELR designs incorporate such a high SL percentage that the
15 contribution of the elastomeric portion to the self-assembly process is imperceptible^{27,28}. However,
16 experience with SELR designs with a lower SL content has demonstrated that, in such compositions, the
17 EL blocks are able to maintain their characteristic thermal transition²⁸⁻³⁰. One of the main drawbacks
18 associated with the use of SL motifs as physical crosslinking domains to obtain injectable hydrogels is
19 that the kinetics of β -sheet formation under physiological conditions (aqueous medium, neutral pH and
20 37°C) is too slow³¹. This is clearly different from the kinetics of ELR self-assembly, which is
21 practically instantaneous above Tt. An interesting example of SELRs explored for their capacity to
22 show dual elastin and silk associations have been reported²⁸. Nevertheless, in that work the ratio SL to
23 EL ranged between 15% to 60% so the portion of SL blocks was high and clearly dominated the self-
24 assembling properties of the molecule giving no much space for exploiting the self-assembling
25 peculiarities of the EL blocks.
26
27
28
29
30
31
32
33
34
35
36
37
38
39
40
41
42
43
44
45
46
47
48
49
50
51
52
53
54
55
56
57
58
59
60

1 The main aim of this work is to test the possibility of combining the two kinds of self-assembly
2 processes to achieve an advanced system in which structure development appears in a multistage and
3 predefined sequence with a major contribution to the self-assembling process of the EL part of the
4 molecule, which in addition will show a more complex amphiphilic molecular architecture and a higher
5 propensity to form stable hydrogels than the previously reported SELRs. Under this general idea we
6 seek to obtain a material that, first, an increase in temperature triggers the assembly of EL- blocks (rapid
7 hydrophobic association), second, the association of the EL blocks triggers the subsequent association
8 of the silk blocks (β -sheet formation) and, simultaneously, fibrillar structures emerge upon maturation
9 of the β -sheet associations.
10
11
12
13
14
15
16
17
18
19
20
21
22

23 A new SELR has been designed, produced, and studied to test this hypothesis. The composition of this
24 SELR is dictated by a reductionist approach in which the minimal structure displaying the desired
25 physical properties is the subject of study, thereby avoiding the incorporation of bioactive domains, that
26 can be added later to fully develop the final functionality of the system. The dynamics of gelation, the
27 interdependence among stages, the mechanical properties of the thus-formed hydrogels, and the
28 structural characteristics at a microscopic and molecular level are reported in this work.
29
30
31
32
33
34
35
36
37
38
39
40

41 **MATERIALS AND METHODS.**

42 **Construction of (EIS)x2 (SELR) and (EI)x2 (ELR)**

43
44
45 Gene synthesis was carried out using standard molecular biology protocols. DNA sequences encoding
46 each monomer were contained in a modified version of the cloning vector pDrive (Qiagen), named as
47 pDAll, characterized by the engineering of two inverted Eam 1104 I and one SapI restriction sites in the
48 poly-linker region. Thus, the DNA sequence encoding each monomer cloned in pDAll vector is flanked
49
50
51
52
53
54
55
56
57
58
59
60

1 by Eam 1104 I and SapI recognition sites in 5' termini and Eam 1104 I site at 3' termini. Sequential
2 introduction of the repetitive EL or SL polypeptide-coding gene segments to form fusion genes with a
3 fully controlled composition and chain length was carried out using a "recursive directional ligation"
4 (RDL) strategy, by using the restriction type II enzymes Eam 1104 I and SapI . The sequences were
5 verified by agarose gel electrophoresis of the restriction fragments generated after enzymatic digestion
6 and automated DNA sequencing. Selected genes were sub-cloned into a modified version of pET-25(+)
7 expression vector.
8
9
10
11
12
13
14
15
16
17
18
19
20

21 **(EIS)x2 production and purification**

22
23

24 The modified version of pET-25(+) expression vector containing our gene construction was transformed
25 into the *E.coli* strain BLR(DE3)star (Invitrogen). The resulting recombinant strain was grown at 37°C in
26 the auto-induction medium (Terrific broth) in a 15L bioreactor (Applikon), reaching optical density
27 values up to 8 at 600 nm after 12 h. Immediately after, cells were recovered by centrifugation at 4°C,
28 and the cell pellets were resuspended in saline buffer prior disruption (Constant Cell Disruption
29 System). The resulting soluble fraction obtained after centrifugation was subjected to the purification
30 steps, The purification protocol consisted of sequential rounds of inverse transition cycling (ITC)
31 optimized according to the specific characteristics of the (EIS)x2 co-recombinamer. The purity and
32 molecular weight of the co-recombinamer were routinely determined by sodium dodecyl sulfate
33 polyacrylamide gel electrophoresis (SDS-PAGE) and mass spectrometry (MALDI-TOF/MS). The
34 amino acid composition was further verified by HPLC analysis. NMR analysis was also carried out in
35 order to ensure the absence of non-proteinaceous organic impurities.
36
37
38
39
40
41
42
43
44
45
46
47
48
49
50
51
52
53
54
55
56
57
58
59
60

Visualization of the sol-gel behavior

In order to check the ability of both recombinamers to rapidly form hydrogels upon increasing the temperature, 15 wt. % aqueous solutions of (EIS)_{x2} and (EI)_{x2} were prepared by dissolving the pure recombinamers in PBS at 4°C for 6 h. Once the recombinamers were in a sol state at 4°C, they were placed at room temperature. After one minute, the samples were inverted and pictures were taken.

A solution of (EIS)_{x2} co-recombinamer at 15 wt. % was loaded into a syringe at 4°C and the tip of the syringe removed with a knife. The syringe plunger was then depressed to deposit the co-recombinamer solution into the aqueous PBS medium at 37°C. In parallel, a solution of (EI)_{x2} co-recombinamer was subjected to the same procedure as negative control. Photographs were taken at different times in order to monitor the evolution of the formed hydrogels.

In order to check the injectability, a 15 wt.% solution of the (EIS)_{x2} co-recombinamer at 4°C was loaded into a syringe and injected into an aqueous PBS solution at 37°C and neutral pH. Needles with diameters ranging from 18G to 23G were used.

Macroscopic properties: Thermal properties

We decided to use the DSC technique to monitor the formation of irreversible physical cross-links in the (EIS)_{x2} co-recombinamer. DSC experiments were performed using a Mettler Toledo 822e with liquid-nitrogen cooler. Both temperature and enthalpy were calibrated with a standard sample of indium. The solutions for the DSC experiments were prepared at 5, 10 and 15 wt.% in an aqueous buffered solution (PBS). 20 μL of the corresponding solution was placed inside a standard 40-μL aluminum pan, sealed hermetically, and subjected to annealing treatments comprising incubation at fixed temperatures (5, 10, 15, 25, 37, 60°C). The samples were analyzed by DSC at different times. The heating program for DSC

1 experiments included an initial isothermal stage (5 min at 0°C for stabilization of the temperature and
2 the state of the recombinamers), followed by heating at 5°C/min from 0°C to the desired temperature
3 range. The same rate was applied for cooling processes. The enthalpy values for endothermic processes
4 were taken as negative and exothermic values as positive.
5
6
7
8

9
10 In order to quantify the progression rate of the irreversible folding mediated by SL blocks, the
11 normalized ratio between the secondary peak (I_2) and the main peak (I_1) was plotted versus time. These
12 curves were fitted to a first-order kinetics, and the rate constant “k” for each annealing temperature was
13 obtained. The temperature-dependence of “k” was analyzed using an Arrhenius equation.
14
15
16
17
18
19

$$20 \quad k = A \cdot e^{-\frac{E_a}{R \cdot T}}$$

21
22 In the above, “k” is the kinetic constant, “A” is the pre-exponential factor, “R” is the Universal gas
23 constant (8.3 J/mol·K), “Ea” is the activation energy (expressed in J/mol), and “T” is the temperature (in
24 kelvin).
25
26
27
28
29
30
31
32
33
34
35
36

37 **Macroscopic properties: Rheology**

38
39 The mechanical properties of the hydrogels were determined using rheological tests in a controlled
40 stress rheometer (AR2000ex, TA Instruments) equipped with a Peltier plate temperature control.
41
42
43
44

45 Conversion of the solution to a gel, known as the sol-gel process, was studied for both (EI)x2 and
46 (EIS)x2. A parallel plate geometry with a diameter of 20 mm and a sample volume of 350µL in PBS
47 was used. The temperature ramp and gelation kinetics were carried out at a constant strain of 0.1% and a
48 frequency of 1 Hz. Temperature ramp experiments were performed in the concentration range 5-15
49
50
51
52
53
54
55
56
57
58
59
60

1 wt.% by heating the sample from 5 to 37°C at a rate of 2.5°C/min; the reverse process (cooling) was
2 performed under the same conditions. The gelation kinetics were measured at 37°C.
3
4

5 The active involvement of the SL blocks in the mechanical performance of the hydrogels was studied.
6 To this end, (EIS)x2 was dissolved at 5, 10 and 15 wt.% at 4°C for 6h, and the resulting solutions placed
7 in a mold, sealed, and incubated at 37°C for a period of 1, 2, 5, and 10 days. After this time the
8 hydrogels (referred to as hydrogels with annealing) were measured in the rheometer at 37°C and 5°C
9 using a parallel plate geometry (20 mm diameter). Measurements of G' (elastic or storage modulus) and
10 G'' (viscous or loss modulus) were performed by varying the frequency (between 0.1 and 10 Hz) in a
11 constant strain mode (0.1%). Bulk elastic modulus “K” was calculated by applying the relation between
12 “G”, “K”, and the Poisson coefficient (ν)³². Poisson coefficient was estimated to be 0.49³³
13 (Supplementary Information).
14
15
16
17
18
19
20
21
22
23
24
25
26
27
28
29
30
31

32 **Molecular level: FTIR analysis**

33 Possible conformational changes in (EIS)x2 due to the annealing treatment were evaluated by FTIR. To
34 this end, an (EIS)x2 hydrogel annealed for 3 days and 5 days at 37°C was dried in an oven at 37°C in
35 order to obtain a film and thus avoid the interference of water with the FTIR measurement. Moreover,
36 since methanol treatment promotes folding in β -sheets, an additional sample, the preparation of which
37 involved annealing for 5 days, similar to the previous sample, and an additional treatment with 70%
38 methanol for two hours, was measured. Freeze-dried pure co-recombinamer without any annealing
39 treatment was also checked as negative control and compared with the (EI)x2 co-recombinamer.
40
41
42
43
44
45
46
47
48
49
50

51
52
53 Fourier Transform Infrared spectroscopy (FTIR) analysis was performed using a Bruker Tensor 27
54 spectrometer. For each measurement, 512 scans were co-added with a resolution of 2 cm⁻¹ in the
55
56
57

1 wavenumber range from 1400 to 1800 cm^{-1} . The statistical significance of the peak shifts observed was
2
3 estimated by a two-way ANOVA followed by Tukey's multiple comparisons test.
4
5
6
7
8

9 **Dynamic Light scattering (DLS)**

10
11
12 Dynamic light scattering measurements were performed using a BI-200SM multiangle goniometer
13 (Brookhaven Instrument, Holtsville, NY) with a 33mW He-Ne vertically polarized laser at a
14
15 wavelength of 632.8 nm and a digital correlator (BI-9000AT).
16
17
18
19

20
21 Solutions of (EI)x2 and (EIS)x2 were prepared by dissolving pure, lyophilized products in MilliQ water
22
23 with 0.05% sodium azide to a concentration of 25 μM . These solutions were kept at 4 $^{\circ}\text{C}$ overnight to
24
25 allow complete dissolution of the proteins. The samples were incubated at 37 $^{\circ}\text{C}$ to allow supramolecular
26
27 assembly to occur, and measured at different time intervals. DLS measurements were performed at a
28
29 scattering angle of 90 $^{\circ}$. Co-recombinamer solutions at a concentration of 25 μM were introduced into
30
31 glass cells and stabilized for 10 min at the fixed temperature (5 or 37 $^{\circ}\text{C}$) in a thermostatted decalin bath.
32
33
34
35

36
37 Volume distributions were determined using a Zetasizer nano ZSP (Malvern Instruments) equipped with
38
39 a 10 mW He-Ne laser at a wavelength of 633 nm. Samples were introduced into polystyrene cuvettes
40
41 and stabilized for 10 min at the desired temperature. Size was obtained from the correlation function, by
42
43 using Cumulant analysis.
44
45
46
47
48
49

50 **Transmission electron microscopy (TEM)**

51
52
53 Nanostructure formation was checked by TEM. Solutions of (EI)x2 and (EIS)x2 were prepared by
54
55 dissolving pure, lyophilized products in MilliQ water to a concentration of 25 μM . These solutions were
56
57

1 kept at 4 °C overnight to allow complete dissolution of the proteins. To prevent biological
2 contamination, azide was added to a final concentration of 0.05% The sample was incubated at 37°C to
3 allow supramolecular assembly to occur, and an aliquot was taken and measured at different time
4 intervals (0, 48 and 96 hours and 7 months). TEM measurements were performed using a JEOL JEM-
5 1230 electron microscope operating at 120 kV. The specimens were prepared by placing a drop of the
6 solution on a plasma-treated carbon-coated copper grid, followed by water evaporation at 37°C.
7
8
9
10
11
12
13
14
15
16
17
18

19 Atomic Force Microscopy (AFM)

20
21
22 Stock solutions of (EI)x2 and (EIS)x2 were prepared by dissolving pure, lyophilized products in PBS to
23 a concentration of 25 μM. These solutions were kept at 4°C overnight to allow complete dissolution of
24 the proteins. To prevent biological contamination, azide was added to a final concentration of 0.05%. A
25 drop (50 μL) of each co-recombinamer at each tested condition (without annealing and with 7 months of
26 annealing at 37°C) was deposited onto a clean graphite (HOPG) surface and dried at 37°C. The dried
27 samples were analyzed using a Multimode 8 AFM attached to a Nanoscope V electronics (Bruker) in
28 tapping mode.
29
30
31
32
33
34
35
36
37
38
39
40
41
42

43 RESULTS AND DISCUSSION.

46 Construction of (EIS)x2 (SELR) and (EI)x2 (ELR)

47
48
49 The amino-acid sequences of the different constructs (EI)x2 and (EIS)x2 used here are, respectively, (1)
50 MESLLP-{{(VPGVG)2-(VPGEG)-(VPGVG)2}10[VGIPG]60}2-V and (2) MESLLP-{{(VPGVG)2-
51 (VPGEG)-(VPGVG)2}10[VGIPG]60)-[V(GAGAGS)5G]2}2-V. (EI)x2 is the control ELR, which has
52
53
54
55
56
57
58
59
60

1 the same EL composition as (EIS)x2 but lacks the SL blocks. The construction and purification of
2 (EI)x2 has already been reported ¹⁴. With regard to (EIS)x2, sequential introduction of the repetitive
3 polypeptide-coding gene segments to form fusion genes with a fully controlled composition and chain
4 length was carried out using the recursive directional ligation (RDL) technique ^{34,35}. DNA sequencing
5 and restriction mapping analysis showed the correctness of the gene-construction process (Data not
6 shown).
7
8
9
10
11
12
13
14
15
16
17
18

19 **(EIS)x2 production and purification**

20
21 (EIS)x2 was successfully purified using by an optimized inverse temperature cycling (ITC) ³⁶ protocol.
22 Production yields of around 170 mg per liter of bacterial culture were achieved. The final product was
23 characterized by SDS-PAGE electrophoresis (Figure S1), MALDI-TOF mass spectrometry (Figure S2),
24 amino acid analysis (Table S1), and NMR spectroscopy (Figure S3), which confirmed the purity and
25 correctness of the biosynthetic process in terms of sequence and molecular mass (See Supporting
26 Information).
27
28
29
30
31
32
33
34
35
36

37 According to the literature, many SELRs have been purified by different methods that invariably
38 comprise a chromatographic step ³⁷. However, chromatography is expensive, requires specialized
39 equipment and is difficult to scale up, therefore alternative protocols are preferred. As such, simplified
40 purification protocols based on the use of acidic pH combined with ammonium sulfate precipitation
41 have been developed ³⁸. Although the stimuli-responsive behavior of ELRs is maintained upon
42 incorporation into a chimeric fusion protein ^{39,40}, such behavior has not been exploited as a feasible
43 option for SELR purification since temperature accelerates the irreversible gelation process mediated by
44 SL folding. Nevertheless, we have successfully made use of the reversible inverse transition of the
45 elastomeric part of (EIS)x2 from soluble to insoluble and, as a result, have managed to purify (EIS)x2
46
47
48
49
50
51
52
53
54
55
56
57
58
59
60

1 using inverse transition cycles. This finding is likely motivated by the proportion of SL blocks to EL
2 blocks used in this construct, which is relatively small (the EL blocks clearly dominate the final
3 structure) compared to other SELRs found in the literature. This method entails a number of advantages,
4 such as low cost and scalability. To the best of our knowledge, this is the first time that a SELR has
5 been purified using such an approach.
6
7
8
9
10

11 **Visualization of the sol-gel behavior**

12
13
14
15
16
17
18
19
20 15% aqueous solutions of both co-recombinamers have demonstrated their ability to rapidly form
21 hydrogels with increasing temperature (Figure 1, a - d). In principle, both co-recombinamers behave the
22 same and display a sol-gel transition as the temperature is increased.
23
24
25
26

27
28 In most physical hydrogels, an excess of water acts as a destabilizing agent for the network of
29 noncovalent interactions, therefore their exposure to fluids is considered to have adverse effects. In our
30 case, upon exposing the two gels to such a detrimental environment, and despite the initial similarities,
31 the two gels display clear differences. To check the stability of (EI)_{x2} and (EIS)_{x2} in the presence of an
32 excess of aqueous medium, 15 wt.% solutions of both recombinamers at 4°C were directly added to an
33 aqueous PBS medium (pH 7) at 37°C, as described in the Experimental Section. As shown in Figure 1 e,
34 after adding the cold solution to the warm aqueous medium, both solutions promptly showed the
35 formation of a hydrogel. However, the stability of these hydrogels with time was clearly different,
36 exhibiting striking differences after incubation for only 1 day under these conditions. Thus, the (EI)_{x2}
37 hydrogel disaggregated completely and no signs of it were evident, with only a slightly turbid solution
38 remaining (Figure 1 f). In contrast, the (EIS)_{x2} hydrogel did not disaggregate but acquired a more
39 robust appearance (Figure 1 g). This latter hydrogel remained stable for at least two months under those
40 conditions (Figure 1 , j) and, from the very beginning and up to the end of the experiment, displayed
41
42
43
44
45
46
47
48
49
50
51
52
53
54
55
56
57
58
59
60

sufficient consistency to be easily manipulated (Figure 1 k). Hydrogel degradation was estimated to be 10% (Supplementary information. Figure S 6).

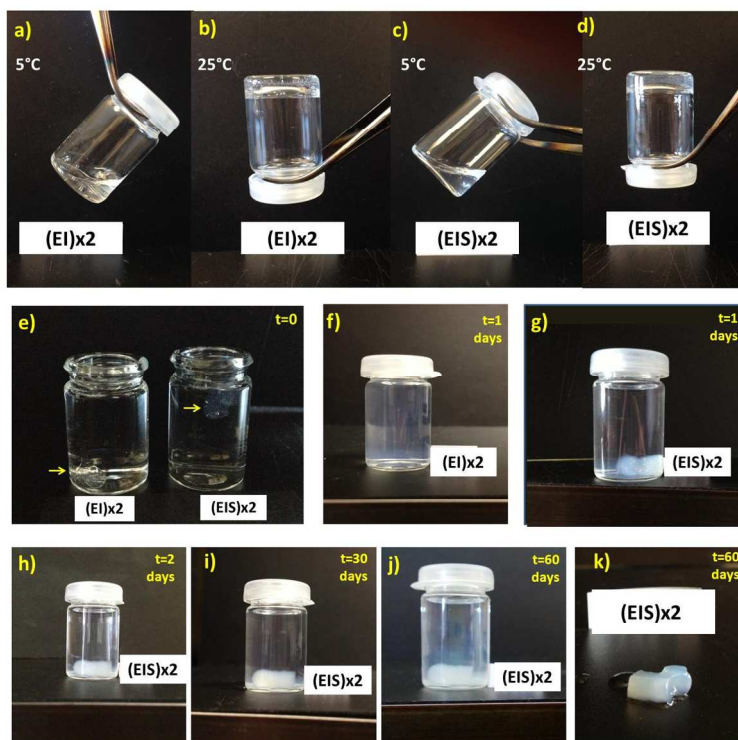


Figure 1: Pictures showing both the ability to rapidly form hydrogels upon increasing the temperature and the stability features of (EI)x2 and (EIS)x2: a) aqueous solution of (EI)x2; b) (EIS)x2 hydrogel formed upon increasing the temperature; c) aqueous solution of (EIS)x2; d) (EIS)x2 hydrogel formed upon increasing the temperature; e) picture taken just after addition of the co-recombinamer solutions to the aqueous medium in a 3 mL glass vial; f) to j) pictures taken at different times after adding the co-recombinamer solutions to the aqueous medium (PBS) in a 3 mL glass vial. k) (EIS)x2 hydrogel removed from the aqueous medium after two months.

The existence of a gelation triggered by a temperature increase suggests the possibility of using these hydrogels, and especially (EIS)x2 due to its increased stability, as injectable systems in minimally invasive therapeutic approaches. As such, the injectability of a 15 wt.% (EIS)x2 solution (in PBS at 10°C) was checked using a battery of needles of different diameters. G18, G19, G21, and G23 needles

1 were tested and it was found that the samples were very easily injected using needles of diameters G18
2 and G19 and they could also be injected without difficulty using a G21 needle. In contrast, injection
3 using a G23 needle was unsuccessful.
4
5
6

7
8 Consequently, all the general properties qualitatively shown above point to the potential of (EIS)_{x2} as a
9 very attractive candidate for use in biomedical applications, where injectability and rapid *in situ* gelation
10 are required, without any restrictions with regard to exposure to fluids.
11
12
13

14
15
16 In order to quantify the behavior observed upon the visual inspection of both gels, their thermal and
17 mechanical properties at the macroscopic level were first studied.
18
19
20

21 22 23 24 25 26 **Macroscopic properties: Thermal properties** 27

28
29 The thermal properties of the hydrogels produced by these materials were studied by DSC. DSC has
30 proven to be an adequate technique to quantify the ITT, providing values for both the T_t and latent heat
31 (ΔH). DSC scans were carried out on both (EIS)_{x2} and (EI)_{x2} solutions, as detailed in Materials and
32 Methods. Figure 2 shows the thermograms for (EIS)_{x2} (a and b) and (EI)_{x2}, which was used as control
33 (c and d). The thermograms labeled with as “0 h” correspond to the thermal behavior found for the
34 freshly dissolved co-recombinamers. The T_ts estimated from the peak temperatures were 14.4°C for
35 (EIS)_{x2} and 13.0 °C for (EI)_{x2}, and the associated enthalpies for such ITTs were 8.2 and 9.1 J/g,
36 respectively. The presence of the hydrophilic amino acid serine in the sequence of the SL motif could be
37 responsible for the observed increase in T_t and subsequent decrease in enthalpy of (EIS)_{x2} with respect
38 to (EI)_{x2}. According to the literature, the ITT of the hydrophobic block (VGIPG) in (EI)_{x2} leads to a
39 gel state¹⁴. Such gelation is fully reversible since the sol state is recovered simply by lowering the
40 temperature below its T_t. The similarity in terms of T_t and enthalpy values, and the similarity of their
41
42
43
44
45
46
47
48
49
50
51
52
53
54
55
56
57
58
59
60

1 shapes, leads us to conclude that, for the freshly dissolved solutions, (EIS)_{x2} presumably experiences a
2 thermogelling process similar to that displayed by the control (EI)_{x2}, with the effect of the SL block
3 being restricted to a modest shift in the T_t and ΔH values. Moreover, the reversibility of the measured
4 thermodynamic process provides further evidence for the correspondence of such process with the ITT
5 of the (VGIPG) blocks present in (EIS)_{x2} (Figure 2, a and b).
6
7
8
9
10

11
12
13 However, when used as an implantable system, this hydrogel will be subjected to a relatively prolonged
14 isothermal state at 37°C during its service time. Therefore, to determine whether the system can
15 experience a change in properties during that period, a set of samples annealed at 37°C for different
16 times were also studied by DSC. The changes in the shape of the thermogram for (EIS)_{x2} are evident
17 and dependent on the annealing time. Thus, after incubation at 37°C for 15 h, the endothermic peak
18 becomes broader and is characterized by the incipient appearance of a shoulder or secondary endotherm
19 at lower temperatures. At longer annealing times the shape of the endotherm evolves further and the
20 presence of the secondary peak at a temperature of 11.0°C becomes increasingly clear. After annealing
21 at this temperature for 63 h the new peak at 11.0°C becomes the main one, leaving only a slight trace of
22 the peak previously seen at 14.4°C. From 87 h on, the shape of the thermogram appears to remain
23 unchanged. These results contrast with the behavior of (EI)_{x2}, which exhibited neither peak broadening
24 nor the appearance of a secondary peak at any annealing time (Figure 2, c and d).
25
26
27
28
29
30
31
32
33
34
35
36
37
38
39
40
41

42 On the other hand, the endothermic peak and its associated ITT measured for each annealing time were
43 totally reversible and, in a heating-cooling cycle, the endothermic peak transformed into an exothermic
44 peak with an identical ΔH and only minor differences in T_t that can easily be explained on the basis of
45 the thermal lag of the experimental setup. Moreover, on cooling, this exothermic peak displayed the
46 same shape as its counterpart endothermic peak for each fixed condition (co-recombinamer and
47 annealing time). Such reversibility further reinforces the association of these endotherms in heating and
48 their corresponding cooling exotherms with the EL-block ITT. In addition, since the only difference
49
50
51
52
53
54
55
56
57
58
59
60

1
2
3
4
5
6
7
8
9
10
11
12
13
14
15
16
17
18
19
20
21
22
23
24
25
26
27
28
29
30
31
32
33
34
35
36
37
38
39
40
41
42
43
44
45
46
47
48
49
50
51
52
53
54
55
56
57
58
59
60

between (EI)x2 and (EIS)x2 is the presence of SL blocks in the latter, it can be concluded that the variation in the shape of the thermogram, which occurs with increasing annealing time at 37°C, must be caused by the presence of this block, which somehow exerts an influence on the ITT.

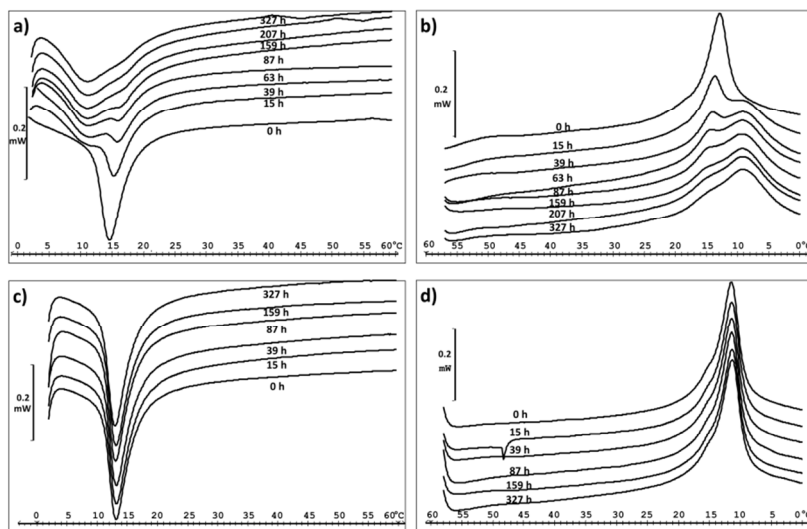


Figure 2: DSC scans for 15 wt.% (EIS)x2 and (EI)x2 solutions after annealing at 37°C for different times. (a) DSC thermograms for heating and (b) cooling processes for (EIS)x2 after annealing at 37 °C for 0, 15, 39, 63, 87, 159, 207 and 327 h. Note the variation in the thermogram shape along annealing time. (c) DSC thermogram for heating and (d) cooling processes for (EI)x2 co-recombinamer solution after annealing at 37 °C for 0, 15, 63, 87, 159, and 327 h. For (EI)x2, thermogram shape remained unchanged.

It can be concluded that annealing at 37°C causes the (EIS)x2 gel to split into a bimodal state. Annealing causes the emergence of a new state in (EIS)x2 that is characterized by a lower Tt. At a molecular level, this must mean that EL blocks in such a state exhibit a lower effective mean polarity, as can be deduced

1 by the shift in T_t to lower values⁴¹. Although both states seem to coexist, the increase in annealing time
2
3 seems to promote growth of the state with lower T_t at the expense of the initial one.
4
5
6
7
8

9 **Macroscopic properties: Rheology**

10
11
12 Macroscopic observation of the systems clearly indicated that freshly prepared solutions of both co-
13
14 recombinamers undergo a rapid gelation process upon increasing their temperature above their T_t .
15
16

17 Early gelation due to the thermally triggered transition of the (VGIPG) blocks.

18
19
20
21 In order to quantify the resulting mechanical properties, freshly prepared 15 wt.% (EI)x2 and (EIS)x2
22
23 (no annealing) solutions were subjected to a rheological study consisting of heating from 5 to 37°C at a
24
25 rate of 2.5°C/min.
26
27

28
29
30 Many criteria have been used in the literature to estimate the gel point^{14,42,43}. The crossover between G'
31
32 and G'' is usually considered to indicate the gelation point⁴³. However, the crossing point depends on
33
34 the frequency of the oscillatory experiment and, as a consequence, might be close, but not identical, to
35
36 the T_t ⁴⁴. As such, the gel point was estimated here as the temperature where $\tan\delta$ shows a peak since
37
38 such a peak is a direct consequence of the molecular rearrangement of the co-recombinamers due to
39
40 their characteristic ITT.
41
42

43
44
45 As shown in Figure 3 (a and c), gel formation unequivocally occurred for both samples in the
46
47 temperature range from 10°C to 20°C, which is evident for both the G', G'' and $\tan\delta$ plots. The
48
49 maximum storage moduli displayed were $1.1 \cdot 10^3$ Pa and $2.5 \cdot 10^3$ Pa for (EI)x2 and (EIS)x2,
50
51 respectively. When a cooling ramp from 37°C to 5°C was applied to the same samples, the shear
52
53 modulus decreased, reaching values close to 0 Pa at 5°C (Figure 3 b and d). This reversibility of the
54
55
56
57

1
2
3
4
5
6
7
8
9
10
11
12
13
14
15
16
17
18
19
20
21
22
23
24
25
26
27
28
29
30
31
32
33
34
35
36
37
38
39
40
41
42
43
44
45
46
47
48
49
50
51
52
53
54
55
56
57
58
59
60

gelation process is in agreement with the fact that the increase in modulus was a consequence of the reversible transition of the EL block (VGIPG). The observed increase in the storage modulus indicates that, although they were not responsible for this reversible gelation, SL motifs did have an effect on the final characteristics of the hydrogel formed as a result of the reversible transition of the elastomeric portion.

The values of the loss factor ($\tan\delta$) showed a maximum at 13.0°C and 15.8°C for (EI)x2 and (EIS)x2, respectively, and such values would be considered to be representative of the transition from liquid to gel determined by rheological methods⁴⁵, since EL moieties undergo conformational changes from an extended state to a folded one as the ITT takes place. These molecular rearrangements are associated with energy loss in the form of heat. This energy loss is reflected as the subsequent emergence of a peak in the loss factor. It is worth noting that such values are close to the T_t values measured by DSC (13.0 and 14.4°C for (EI)x2 and (EIS)x2, respectively).

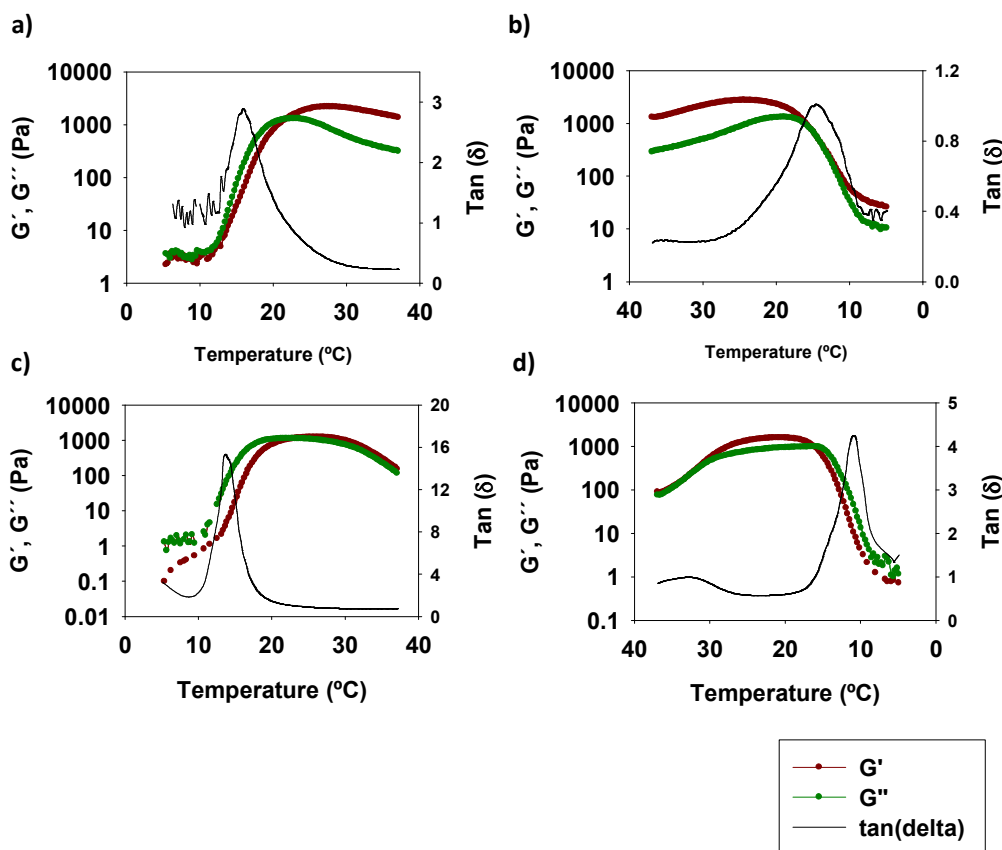


Figure 3: Storage moduli, loss moduli and $\tan\delta$ (G' , G'' and $\tan(\delta)$) for (EI)x2 and (EIS)x2 co-recombinamer solutions (15 wt.%) as a function of temperature: (a) (EI)x2 during heating; (b) (EI)x2 during cooling; (c) (EIS)x2 during heating; (d) (EIS)x2 during cooling. The samples were heated/cooled at 2.5°C/min in the temperature range from 5 to 37°C. Reversible gel formation occurred for both recombinamers in the temperature range from 10°C to 20°C.

The effect of concentration on the reversible thermally triggered gelation process was evaluated by measuring the mechanical properties. To this end, in addition to the already measured 15 wt.% co-recombinamer solutions, 5 wt.% and 10 wt.% (EI)x2 and (EIS)x2 solutions were subjected to heating/cooling cycles (Table 1). In the case of (EIS)x2, for the 10 wt.% concentration and in the temperature range from 10 to 20°C, the formation of a hydrogel took place with a storage modulus of 150 Pa, which is substantially lower than that obtained for the concentration of 15 wt.%. No gelation was observed for the 5 wt.% solution. No gelation was observed for 5 wt.% and 10 wt.% (EI)x2 solutions, which contrasts with the behavior of the (EIS)x2 co-recombinamer, which was able to gel at 10 wt.%. These differences between (EI)x2 and (EIS)x2 again point to an influence of the presence of the SL block in the early gelation process triggered by the EL blocks (VGIPG).

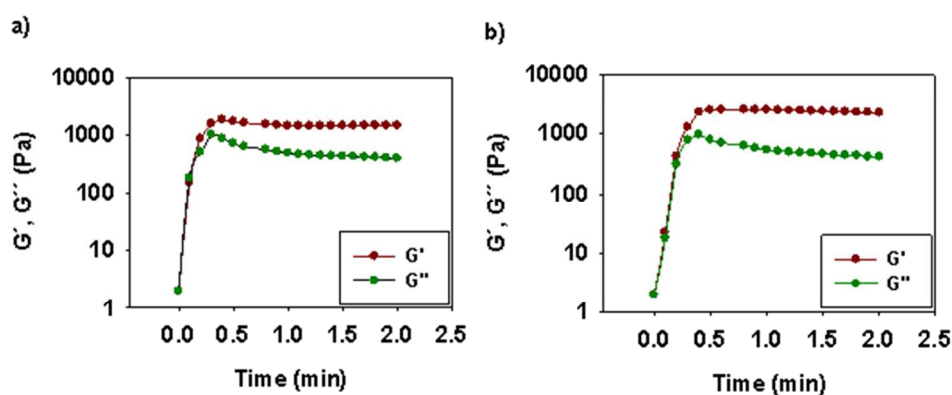
Table 1: Properties displayed by the (EI)x2 and (EIS)x2 reversible hydrogels according to the co-recombinamer concentration. Blank cells indicate no gel formation.

Co-recombinamer	Concentration (%)	T _{gel}	G'_{\max}	G''_{\max}
(EI)x2	5	-	-	-
	10	-	-	-

	15	13.9	1100	430
(EIS)x2	5	-	-	-
	10	15.3	150	70
	15	15.8	2500	550

It was therefore concluded that the ITT of the elastomeric part of (EI)x2 and (EIS)x2 leads to the rapid and early formation of a hydrogel, although the presence of SL blocks exerts an indirect influence on such reversible temperature-triggered gelation.

Once the reversible nature of the thermogelling process experienced by both recombinamers had been confirmed, the gelation time was estimated by rheological methods by application of an isotherm at 37 °C to a sample initially kept at 5 °C. As shown in Figure 4, the gelation time at 37°C was less than 30s for both co-recombinamer solutions. Since the solutions were able to form a gel within such a short period, both materials are potential candidates for use as injectable hydrogels. Moreover, such a short gelation time would presumably avoid leaking events once the biomaterial is injected, with the consequent advantages for its application, such as a reduction in losses and misallocation of active components, with a concomitant improvement in treatment efficacy.



1 **Figure 4:** Isotherms for both co-recombinamer solutions at 37 °C. (a) (EI)x2 at 15 wt.% and (b) (EIS)x2
2 at 15 wt.%. Note the sharp increase in G' and G'' values, indicating that the gelation time was less than
3 30 s for both recombinamer solutions.
4
5
6
7
8
9

10
11 Late gelling mediated by the presence of the SL block: Influence of annealing time on the mechanical
12 properties of the hydrogels
13
14

15
16
17 Although the mechanical properties of (EI)x2 do not change with annealing time (results not shown),
18 (EIS)x2 hydrogels display a clear increase in mechanical properties with annealing time. Rheological
19 studies on (EIS)x2 hydrogels with annealing times of 1, 2, 5 and 10 days at 37°C were performed and
20 the results compared with those for the hydrogels without any annealing treatment. As can be seen from
21 Figure 5, an increase in annealing time at 37°C was accompanied by an increase in the mechanical
22 properties (G' and G'') at both measurement temperatures (5 and 37°C). Such increase in the
23 mechanical properties agrees with the previously visualized gelation process (Figure 1). Moreover,
24 irrespective of the presence of SL blocks, the EL part remained able to respond to the temperature
25 variation, as reflected in the decrease in the moduli (G' and G'') upon lowering the temperature from
26 37°C to 5°C (Figure 5). These results were consistent with our initial hypothesis that, at 37°C, both
27 elastomeric and SL blocks are involved in crosslinking of the hydrogels with annealing. Lowering the
28 temperature of the hydrogels to 5°C would exclude the effect of crosslinking by the elastomeric
29 (VGIPG) motifs, thereby explaining the observed reduction in the moduli.
30
31
32
33
34
35
36
37
38
39
40
41
42
43
44
45
46
47
48
49
50
51
52
53
54
55
56
57
58
59
60

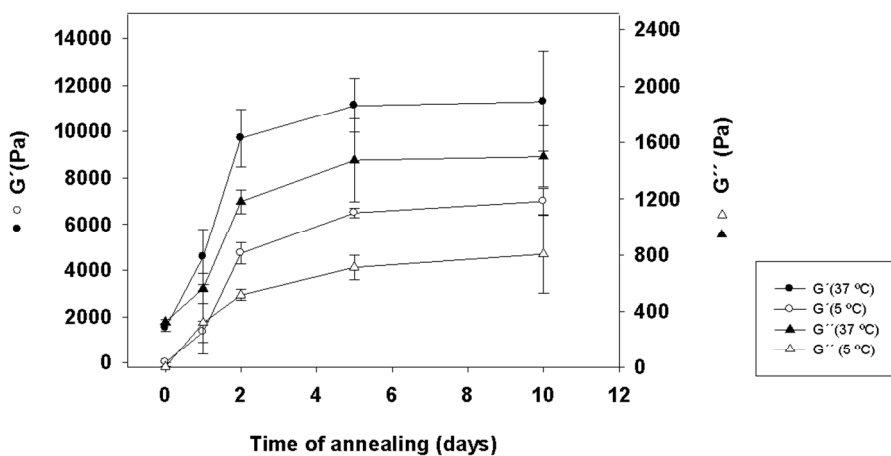
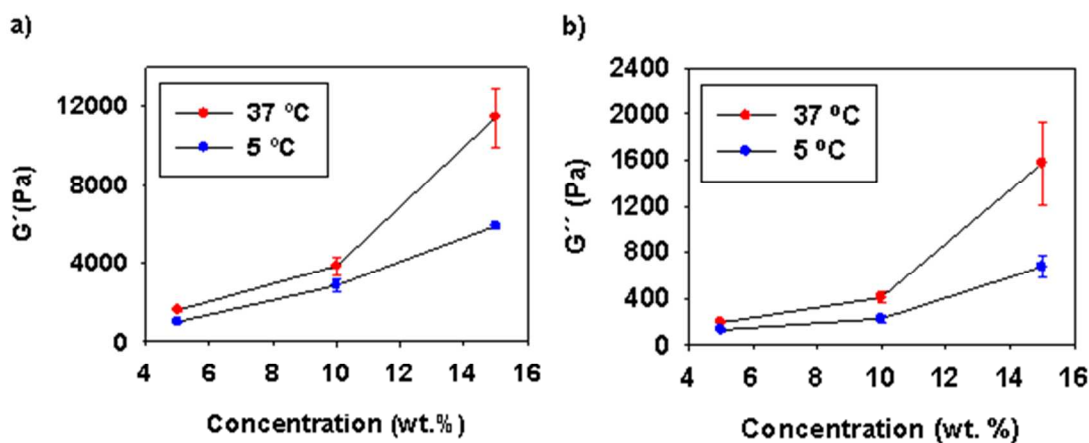


Figure 5: Rheological properties for (EIS)x2 hydrogels measured at 5°C and at 37°C with different annealing times at 37°C. The data shows an increased in the mechanical properties at both temperatures as the annealing time is increased.

As expected, the mechanical properties displayed by the (EIS)x2 hydrogels are concentration-dependent (Figure 6). This is true for both fresh and annealed samples under all annealing conditions. As an example, the values for an annealing time of 5 days are plotted in Figure 6. The G' and G'' values for that annealing time for 5 wt.%, 10 wt.%, and 15 wt.% (EIS)x2 samples showed the expected increase in G' and G'' as a function of concentration. It should be noted, however, that the trend shown by the shear modulus is not linear. The increase in G' and G'' (slope of the curves in Figure 6) is higher for higher concentrations, thereby indicating that the increase in modulus is not just the proportional consequence of the increase in mass of the solid phase of the hydrogel.



1
2
3 **Figure 6:** Representation of G' (a) and G'' (b) for (EIS)x2 hydrogels annealed at 37°C at different
4 concentrations. The measurements were carried out at 5 °C and at 37 °C. Note the increase in G' and
5
6
7
8
9 G'' values at both temperatures with increasing the concentration.

10
11 In conclusion, the rheology tests performed demonstrate that the (EIS)x2 hydrogel exhibits a dual
12 gelling behavior. Thus, (EIS)x2 undergoes an early gelation due to the reversible ITT of the (VGIPG)
13 block and then experiences an increase in its consistency as a result of annealing. As the only difference
14 between the two materials is the presence of SL blocks in the (EIS)x2, this later maturation must be
15 caused by these blocks. The following group of experiments is aimed at gathering information at a
16 molecular and microscopic level to unveil the molecular and structural events that give rise to the
17 macroscopic properties described above.
18
19
20
21
22
23
24
25
26
27
28
29
30
31
32

33 **Molecular level: FTIR analysis**

34
35

36 An FTIR analysis was performed to detect whether the changes experienced by the (EIS)x2 co-
37 recombinamer with annealing time and the previously described macroscopic observations are related to
38 changes in the conformational state of the molecule. IR spectra were obtained (as described in Materials
39 and Methods Section) for samples annealed at 37°C for different times in order to determine whether
40 the maturation process on annealing could also be related to molecular events. The FTIR spectra
41 obtained are shown in Figure 7. The region of the infrared spectrum between 1600 and 1700 cm^{-1} is
42 assigned to the amide I vibration of the peptide backbone⁴⁶⁻⁴⁸. This amide I region corresponds to the
43 C=O stretching vibration, which is directly related to the secondary structure of the protein backbone
44 and is commonly used for the quantitative analysis of different secondary structures⁴⁹. Annealed
45
46
47
48
49
50
51
52
53
54
55
56
57
58
59
60

(EIS)x2 samples underwent a shift of the amide I band towards the 1600-1640 cm^{-1} region with respect to the control (unannealed (EIS)x2). Thus, while the peak for both (EI)x2 and (EIS)x2 without annealing is found at 1626 cm^{-1} , that for (EIS)x2 shifts towards lower wavenumbers (1624 cm^{-1}) after annealing for three days. This shift is more pronounced for the sample annealed for five days (1620 cm^{-1}). This difference is significant ($p < 0.01$). According to the literature, the region between 1600 and 1640 cm^{-1} is related to the presence of β sheets⁴⁸. The signals that appear in the region 1640-1660 cm^{-1} are associated with the presence of random coils and α -helices. The remaining parts of the spectra (1660-1690) are dominated by vibrations due to β -turn structures⁴⁸. Consequently, the observed shift in frequency between the control and annealed samples is indicative of the formation of β -sheet structures⁴⁸.

On the other hand, methanol treatment has been reported to promote the formation of β -sheets^{50,51}. However, no significant differences were detected between the sample annealed for 5 days and that annealed for 5 days plus methanol treatment. Therefore, methanol treatment did not further increase the displacement of the amide I band toward the region 1640-1600 cm^{-1} , thereby indicating that β -sheet formation reaches a maximum extension simply by annealing. This fact was also supported by the DSC experiments and rheological measurements, with no further changes being detected after annealing for five days at 37°C, thus showing that the maturation phase had reached stability.

In light of these results, it is evident that the macroscopic differences found between (EI)x2 and (EIS)x2 are likely caused by the SL block and, more precisely, by its tendency to form β -sheets. As they are based on hydrogen bonding, β -sheets provide stronger, more stable, and less dynamic physical cross-links than those found in a flexible network built exclusively on hydrophobic contacts. The double peak found in the DSC endothermic peak upon heating must therefore be understood as the result of an increase in the hydrophobic environment of the EL blocks directly linked to SL blocks already incorporated into β -sheets. β -sheet formation causes a change in the peptides involved, shifting from a

1 water-soluble to a water-insoluble state. This reflects a decrease in the effective hydrophilicity of the SL
2 blocks after incorporation into the β -sheet structure and, therefore, as they are coupled to the EL blocks,
3 a decrease in the mean hydrophilicity of the (EIS)x2 molecule as a whole. Additionally, formation of the
4 β -sheet structures could also somehow disconnect the hydrophobic EL blocks from the hydrophilic
5 ones. In any case, both effects would cause T_t to decrease, as observed.
6
7
8
9
10

11
12
13 In light of the previous results, it is important to question whether the presence of such β -sheets has any
14 consequences, in terms of structure growth, at the nanometric and micrometric level. The following set
15 of experiments were designed to explore these effects.
16
17
18
19
20
21

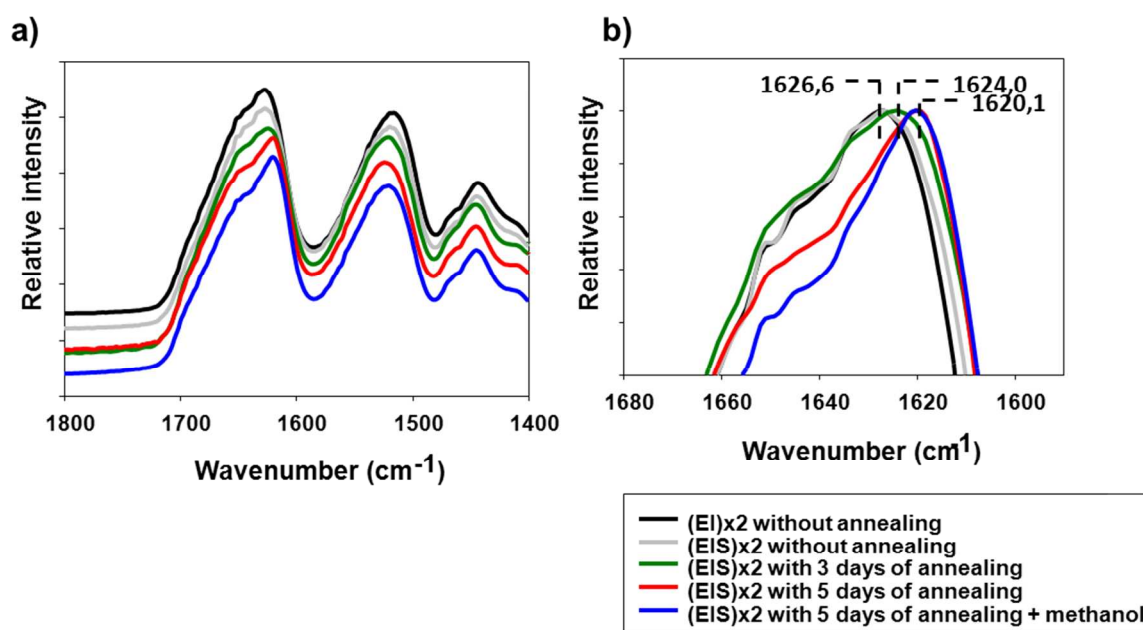


Figure 7: FTIR absorbance spectra of (EIS)x2 samples: a) FTIR spectrum of amide I and amide II region; b) magnified view of the peaks in the amide I region. Grey: Untreated (EI)x2. Black: Untreated (EIS)x2. Green: (EIS)x2 after annealing for three days. Red: (EIS)x2 after annealing for five days. Blue:

1 (EIS)_{x2} after annealing for five days and treatment with methanol for two hours. The shift towards
2 lower wavenumbers with increasing annealing time is indicative of the formation of β -sheets.
3
4
5
6
7
8

9 **Dynamic Light Scattering**

10
11
12
13 Dynamic Light Scattering (DLS) was performed in order to check whether characteristic and differential
14 self-assembled nanostructures were formed by the recombinamers studied as a consequence of an
15 increase in temperature above and below T_t and also when annealed at 37°C at different times. DLS
16 measurements were carried out using dilute samples so as to provide information on the basic structural
17 elements that might form as a consequence of potential self-assembly processes triggered by the
18 formation of hydrophobic contacts and β -sheets.
19
20
21
22
23
24
25
26
27

28 Figure 8 shows the intensity measurements obtained for samples at 5 and 37°C (below and above T_t)
29 for both recombinamers after annealing at 37°C for different times. As regards (EI)_{x2} without
30 annealing, no nanostructure is detected at 5°C, whereas an increase in intensity is observed upon
31 increasing the temperature to 37°C, thus indicating the presence of scattering particles. However, as the
32 annealing time increases, the intensity of (EI)_{x2} remains unchanged for at least 7 months, thereby
33 providing evidence for the high stability of these particles and their independency on annealing. In
34 contrast, (EIS)_{x2} exhibits an increase in intensity at both temperatures (5 and 37°C) with increasing
35 annealing time at 37°C. This increase is not progressive and is more pronounced at shorter annealing
36 times (first week), finally stabilizing from 28 days onwards (Figure 8), remaining stable for at least 7
37 months. Interestingly, the evolution of intensity with annealing time (Figure 8) seems to follow the
38 same trend as that shown by the progression of the rheological properties (Figure 5), although the
39 stabilization time is considerably higher for the DLS experiments. This is most likely due to the
40 different concentrations used for both techniques (much lower for the DLS experiments).
41
42
43
44
45
46
47
48
49
50
51
52
53
54
55
56
57
58
59
60

A temperature change from 5 to 37°C has a clear effect on intensity for the studied annealing time in all cases (Figure 8). The intensity increase observed upon increasing the temperature from below to above T_t for in (EIS)x2 has a similar value (22.82 ± 2.12 a.u.) to that displayed by (EI)x2 (18.86 ± 0.35 a.u.), thereby indicating that the transition of the elastomeric part remains operational during the whole annealing period studied at this concentration (25 μ M).

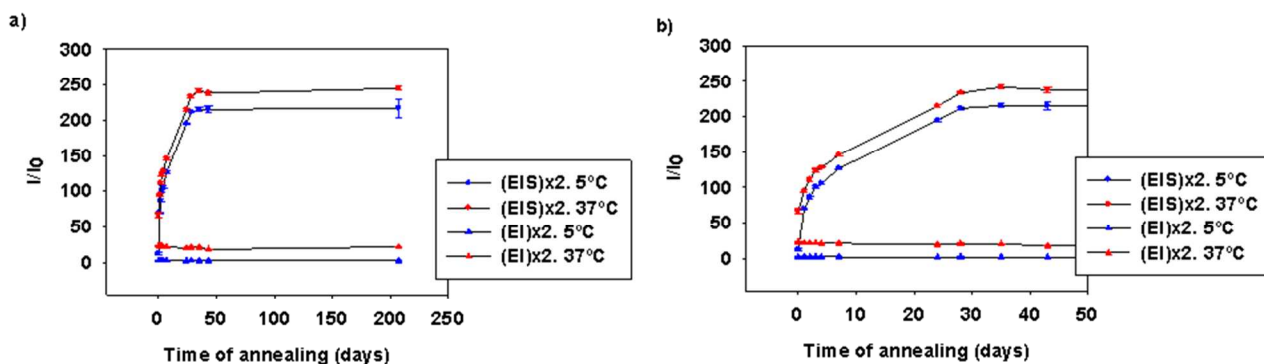


Figure 8: Variation in relative scattered light intensity with annealing time for (EI)x2 (triangles) and (EIS)x2 (circles). B) Magnified view of the first 45 days of annealing. Measurements were carried out at 5°C (blue) and 37°C (red). The graph indicates an increase in intensity with increasing annealing time until stabilization is achieved from 28 days onwards.

The particle-size and volume distributions for both recombamers at two different temperatures (5°C and 37°C) are shown in Figure 9. (EI)x2 nanoparticles with a diameter of 35 nm are formed upon increasing the temperature from 5 to 37°C for both a fresh solution (without annealing) and the sample annealed for a long time (7 months). Intermediate annealing times also showed the same particle size (result not shown), thereby indicating the long-term stability of these particles as well as their lack of evolution. The polydispersity values of 0.05 obtained indicate a low variation in particle size under those conditions for (EI)x2. Nanoparticles of a similar size to those formed by (EI)x2 were detected for (EIS)x2 under non-annealing conditions and at 37°C. However, the major difference arising as a result of annealing at 37°C can be seen from the size distribution, which adopts a clearly different and more

1
2
3
4
5
6
7
8
9
10
11
12
13
14
15
16
17
18
19
20
21
22
23
24
25
26
27
28
29
30
31
32
33
34
35
36
37
38
39
40
41
42
43
44
45
46
47
48
49
50
51
52
53
54
55
56
57
58
59
60

complex profile, thereby pointing to the existence of a more heterogeneous population, with higher polydispersity values of 0.3.

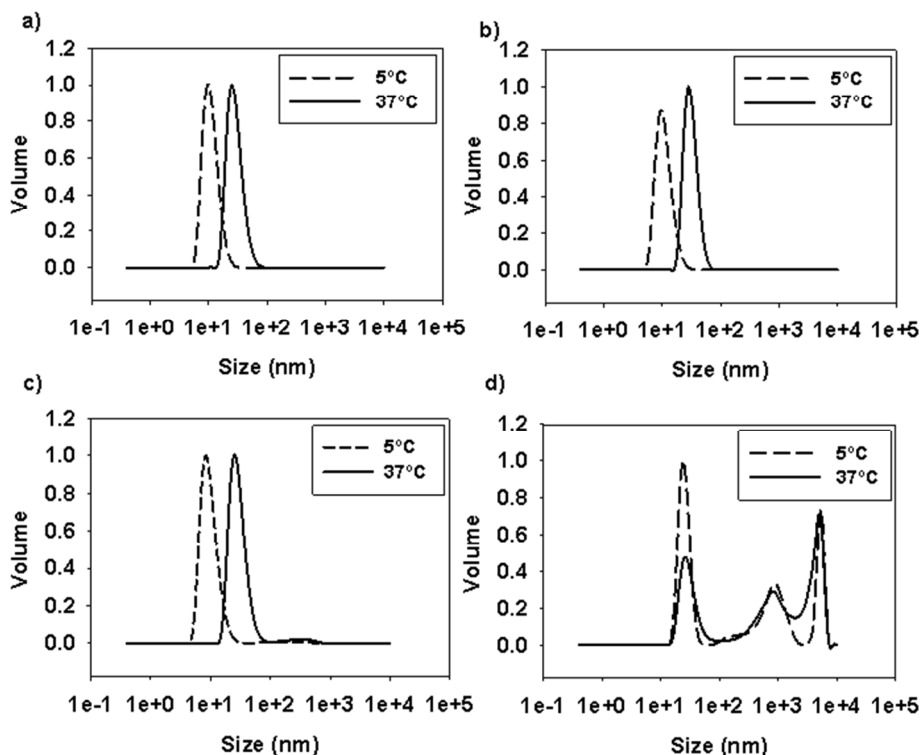


Figure 9: Volume distributions measured at 5 and 37°C for (EI)x2 and (EIS)x2 without annealing and after annealing for 7 months at 37°C: a) (EI)x2 without annealing; B) (EI)x2 after annealing for 7 months; c) (EIS)x2 without annealing; d) (EIS)x2 after annealing for 7 months. Results show that (EI)x2 volume profile remains unchanged after annealing, whereas (EIS)x2 adopts a more complex profile, suggesting the presence of a more heterogeneous population.

In light of the above, the differential evolution found initially at the macroscopic level, and subsequently at the molecular level for both co-recombinamers has a parallel at the nanometric level. As deduced from the DLS measurements, annealing causes substantial changes in the geometrical characteristics of

1 the emerging structures resulting from the two self-assembly processes existing in these samples, i.e.,
2 hydrophobic associations in both co-recombinamers and β -sheet formation in (EIS)x2.
3
4
5
6
7
8

9 **Microscopic observation**

10
11
12 Transmission electron (TEM) and atomic force microscopy (AFM) were used to visualize the structures
13 suggested by the previous LS studies. The TEM images for (EI)x2 indicate the ability of this co-
14 recombinamer to form spherical nanoparticles. The ability of this kind of amphiphilic ELRs to form
15 micelles and spherical vesicles has previously been reported for closely related di- and triblock co-
16 recombinamers⁵²⁻⁵⁴ and other ELRs^{55,56}. The topographical features of these (EI)x2 nanoparticles
17 remain unchanged despite increased incubation at 37°C (Figure 10, a) to d)). These findings are in
18 agreement with the DLS measurements, which showed that the scattering patterns were stable for at
19 least 7 months.
20
21
22
23
24
25
26
27
28
29
30
31

32
33 The TEM images of (EIS)x2 reveal the emergence along annealing of an additional and different
34 structure. Thus, (EIS)x2 is able to self-assemble into nanofibers. The formation of such fibrillar
35 structures is not, however, immediate. In agreement with the DLS data, the only structures found for the
36 freshly prepared solution (no annealing) are micelles. However, fibers start to appear over time (Figure
37 10, e) to h)) and their population increases with annealing time at the expense of the micelle population.
38 At intermediate annealing times, the co-existence of both populations is evident (see for example Figure
39 10f). The mutual presence of micelles and fibers would be in agreement with the behavior found in DSC
40 (Figure 1a and b). Finally, after 96 h at 37°C, a dense network of nanofibers is present; micelles can no
41 longer be visualized and the formed fibers are still present for up to at least 7 months (Figure 10h). Fiber
42 diameter distribution is shown in Figure S 8 (Supplementary information).
43
44
45
46
47
48
49
50
51
52
53
54
55
56
57
58
59
60

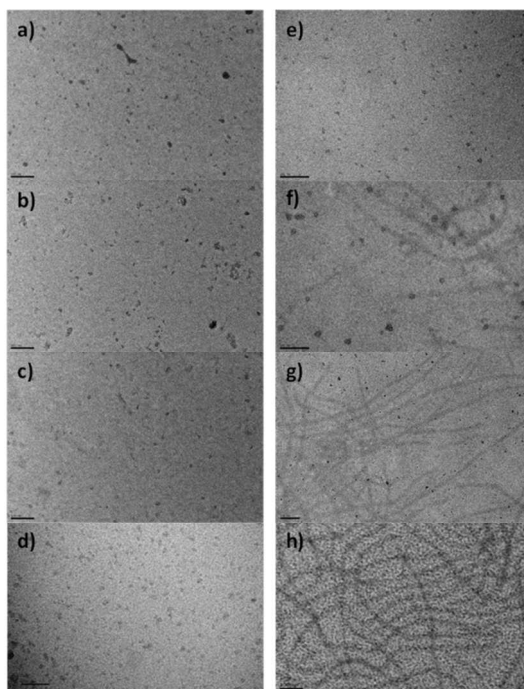


Figure 10: TEM images of the self-assembled nanoparticles formed by (EI)x2 (left) and (EIS)x2 (right) after different annealing times: A) and E) 0 h at 37°C; B) and F) 48 h at 37°C; C) and G) 96 h at 37°C; D) and H) Seven months at 37°C. Images show that (EIS)x2 evolves from a micellar to a fiber-like state. On the contrary, (EI)x2 invariably displays a spherical shape. Scale bar: 100 nm.

AFM was used to further observe and confirm such different morphologies. As shown in Figure 11, (EI)x2 forms spherical nanoparticles at 37°C under both conditions (without annealing and after annealing at 37°C for 7 months). In contrast, (EIS)x2 initially self-assembles into spherical nanoparticles but, after long annealing times, subsequently adopts a fibril shape. These data corroborate the results obtained by DLS and TEM analysis. Interestingly, some of these images may provide clues as to the mechanism of transformation of the micellar structures into fibers. In Figure 11 c, which was obtained for a freshly prepared (EIS)x2 solution (no annealing), the main structural feature is micelles but the alignment of some of these micelles seems to be occurring prior to the fusion and reorganization of the

1 aligned micelles into fibers. The detailed molecular events taking place during this structural transition
2 are intriguing and deserve further study.
3

4
5
6 Therefore, as can be concluded from the microscopic observations, (EIS)x2 ultimately self-assembles
7 into a nanofibrillar morphology in an annealing time-dependent manner. These results are in agreement
8 with the DLS measurements. Taking the DLS and TEM/AFM results together, there is clear evidence
9 that the increase in the presence of these fibril structures with increasing annealing time results in the
10 observed increase in scattering intensity, size distribution profiles, and polydispersity for (EIS)x2 in the
11 bulk state.
12
13
14
15
16
17
18
19

20
21 Other SELRs have been reported to form nano-objects with different shapes, ranging from nanoparticles
22 to nanofibers, depending on the conditions and the SL to EL ratio ^{28,57,58}. Along with the reported
23 evidence for other SELRs and their ability to spontaneously form fibers, and considering that the only
24 difference between (EI)x2 and (EIS)x2 is the presence of SL blocks in the latter, it can be concluded
25 that these blocks are responsible for the ability of these materials to eventually organize into fibrils
26 under the conditions studied. Such nanofibrillar structure resembles those present in the natural ECM.
27
28 Therefore, (EIS)x2 has proven to be able to display a complex and orchestrated self-organization
29 process initially based on a rapid gelation, which is structurally based on bridged micelles and finally
30 evolves into a fibrillar structure. It is noteworthy that such fibrillar structures emerge from a previous
31 micelle-based hydrogel rather than from a solid precipitate, as is common in other fiber-forming
32 polypeptides ⁵⁹.
33
34
35
36
37
38
39
40
41
42
43
44
45
46
47
48
49
50
51
52
53
54
55
56
57
58
59
60

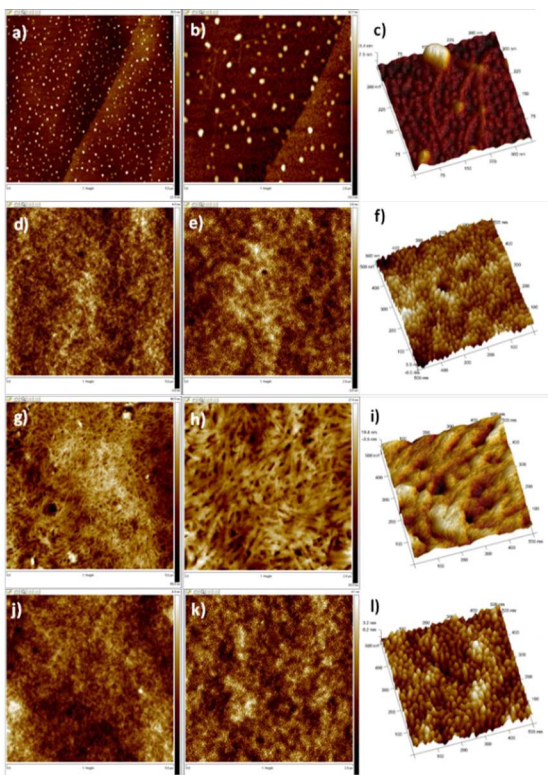


Figure 11: Representative AFM images of the nanostructures derived from (EIS)_{x2} and (EI)_{x2} deposited on an HOPG surface: a) to c) (EIS)_{x2} without annealing. Micellar nanostructures are the predominant population although incipient fibers are discerned. Scanning windows are 5x5 μm , 2x2 μm and 0.5x0.5 μm respectively; d) to f) (EI)_{x2} without annealing. Images indicate the presence of micellar-like nanoparticles. Scanning windows are 5x5 μm , 2x2 μm and 0.5x0.5 μm respectively; g) to i) (EIS)_{x2} after annealing for 7 months. Images show the formation of a nano-fibrillar network. Scanning windows are 5x5 μm , 2x2 μm and 0.5x0.5 μm respectively; j) to l) (EI)_{x2} after annealing for 7 months. Note that micellar like nanoparticles are still present. Scanning windows are 5x5 μm , 2x2 μm and 0.5x0.5 μm respectively.

Coupling of the two gelling processes

1
2
3
4 Finally, our aim was to determine whether there was any interdependence between the two gelling
5
6 mechanisms displayed by (EIS)x2. Thus, to elucidate whether the folding and fiber-arrangement
7
8 kinetics of the SL motifs present in the (EIS)x2 co-recombinamer was dependent exclusively on the
9
10 temperature or if, by contrast, the conformational state of EL blocks also influenced the folding of the
11
12 SL blocks, a final set of experiments were carried out. The transformation between the micellar gel and
13
14 the fibrous gel is followed by a change in the ratio between the secondary peak (I_2) and the main peak
15
16 (I_1) in the DSC thermograms, assuming that the secondary peak is related to the content of the fibrous
17
18 phase whereas the primary peak corresponds to the micellar phase. Kinetic analyses were carried out for
19
20 the (EIS)x2 sample at different annealing temperatures (5, 10, 15, 25, and 60°C) above and below T_t .
21
22 The I_2/I_1 ratio for the different thermograms obtained at different annealing times for each fixed
23
24 temperature can be seen in Figure 12, a. Using these values in a kinetics analysis showed a suitable fit
25
26 for the k values obtained with the Arrhenius equation at annealing temperatures above T_t (Figure 12,b).
27
28 However, when the whole range of temperatures is analyzed, lower temperatures (5 and 10°C) are
29
30 completely out of trend, displaying much lower values, with a clear step around T_t (Figure 12, b).
31
32 According to these data, the kinetics of the transformation from micellar to fibrous gel is influenced by
33
34 both temperature and the conformational state of the co-recombinamer; more specifically, the folded or
35
36 unfolded state of the EL blocks plays a critical role. Therefore, although the formation of β -sheets and
37
38 the fibrillar structure can, in principle, take place without any contribution from the EL blocks, in
39
40 practice this transformation takes place very slowly. However, prior folding of the EL blocks promotes
41
42 an increase in the rate of fibril formation, clearly indicating how these two, in principle, independent
43
44 molecular events are concomitant and strongly connected. We can hypothesize that such concomitant
45
46 interplay between these two molecular events is facilitated by the spatial approximation of the SL
47
48 blocks caused by the micellation driven by the EL blocks. It is also plausible that the recombinant nature
49
50
51
52
53
54
55
56
57
58
59
60

of (EIS)_{x2}, which means that all the molecules are identical in all aspects, including the regular arrangement of the SL and EL blocks, facilitates this coupling of the two processes. Therefore, interestingly, the folding of the EL block is effectively controlling the subsequent self-organization of the SL blocks, thus meaning that these two processes are, in practice, consecutive and interdependent.

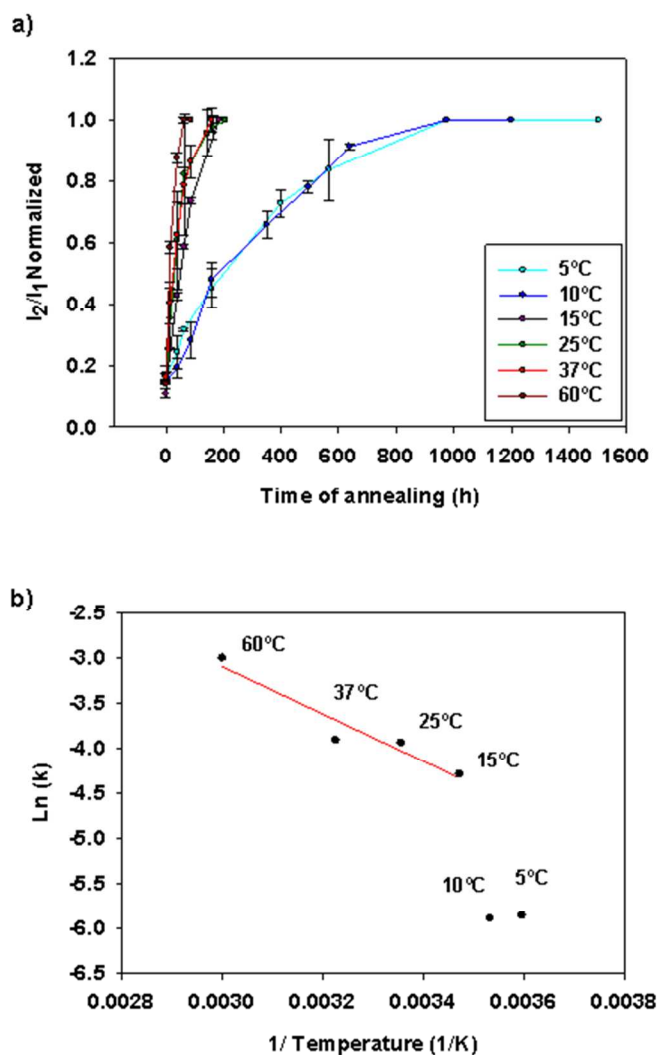


Figure 12: Evaluation of the folding kinetics of SL blocks. a) Representation of the ratio between the secondary peak (I_2) and the main peak (I_1) in the thermograms obtained for (EIS)_{x2} samples after different annealing times at the specified temperatures. b) Representation of the two variables of the

1 Arrhenius equation in order to check the linearity of their dependence. Data show a suitable fit for the
2
3 “k” values obtained with the Arrhenius equation at annealing temperatures above T_t .
4
5
6
7
8

9 CONCLUSIONS

10
11
12 (EIS)x2 is constituted by a combination of EL blocks and SL blocks, with the first ones being already
13 arranged in a tetrablock, thermally triggered, amphiphilic molecule. Another distinctive feature of this
14 composition is that the EL blocks are predominant. As a result of its peculiar composition, this material
15 is able to self-organize from a sol state to a fibrous gel state. This atypical sol-gel transition is
16 characterized by a complex and orchestrated sequence of molecular events displayed by this molecule.
17 This multistage process is initially triggered by an increase in temperature, which induces the self-
18 assembly of the EL blocks as a result of their characteristic ITT. This first step is distinguished by its
19 instantaneity and is dominated by reversible hydrophobic aggregation of the (VGIPG) block. This first
20 stage leads to a soft gel ($G' = 2.5 \cdot 10^3$ Pa) in which a reversible, bridged micellar structure is the main
21 feature. The second stage of this sequence starts at this point: folding of the EL block strongly favors the
22 interaction between the SL blocks and the emergence of irreversible beta-sheet structures. These
23 markedly alter the mode and stability of the hydrogel, which becomes harder ($G' = 1 \cdot 10^4$ Pa). The
24 kinetics of this maturation is slower than that of the first stage. Finally, as a consequence of the
25 maturation of the β -sheet arrangements, the hydrogel gives rise to the emergence of a fibrillar structure.
26 Furthermore, the nanofibrillar architecture adopted by the complex self-organization process of this co-
27 recombinamer emulates the structural organization of the native ECM. In addition, their proven
28 stability, even in environments with a high fluid content, together with their convenient multistage
29 gelation kinetics, makes these hydrogels excellent candidates for use as injectable hydrogels for
30 biomedical applications. This potential is further supported by the excellent properties of ELRs in
31
32
33
34
35
36
37
38
39
40
41
42
43
44
45
46
47
48
49
50
51
52
53
54
55
56
57
58
59
60

1 general. Finally, due to the recombinant nature of this SELR, it is easy to build an extensive –battery of
2 different bioactive versions that can incorporate, at the gene level, relevant peptide-based biological
3 cues such as specific cell-adhesion sequences and metalloprotease recognition sites, amongst others.
4
5 These materials therefore constitute a new versatile family of hydrogels that can be used for many
6
7 different applications and therapies, both *in vitro* and *in vivo*, and may also serve as model artificial
8
9 cellular niches for cell studies and production.
10
11
12
13
14
15
16
17
18

19 SUPPORTING INFORMATION AVAILABLE

20
21
22 SDS-PAGE analysis, MALDI-TOF spectra, amino acid composition for the (EIS)x2, evaluation of the
23 transparency and porous structure by SEM are supplied as Supporting Information. “This material is
24 available free of charge via the Internet at <http://pubs.acs.org>.”
25
26
27
28
29
30
31
32

33 AUTHOR INFORMATION

34 Corresponding Author

35
36
37
38
39
40
41 * E-mail: roca@bioforge.uva.es
42
43
44
45
46

47 Author Contributions

48
49
50
51 The manuscript was written through contributions of all authors. All authors have given approval to
52 the final version of the manuscript.
53
54
55
56
57
58
59
60

ACKNOWLEDGMENT

We acknowledge financial support from the EU through the European regional development fund (ERDF), from the MINECO (MAT2013-41723-R y MAT2013-42473-R, PRI-PIBAR- 2011-1403, and MAT2012-38043), the JCyL (projects VA049A11, VA152A12, and VA155A12), the CIBER-BBN, the JCyL, and the Instituto de Salud Carlos III under the Network Center of Regenerative Medicine and Cellular Therapy of Castilla and Leon.

This work is dedicated to the memory of Prof. Isabel M. Lopez.

REFERENCES

- (1) Zhao, Y.; Sakai, F.; Su, L.; Liu, Y.; Wei, K.; Chen, G.; Jiang, M. *Adv. Mater.* **2013**, *25*, 5215-5256.
- (2) Lutolf, M. P.; Hubbell, J. A. *Nat. Biotechnol.* **2005**, *23*, 47-55.
- (3) Hubbell, J. A. *Curr. Opin. Biotechnol.* **2003**, *14*, 551-558.
- (4) Stevens, M. M.; George, J. H. *Science* **2005**, *310*, 1135-1138.
- (5) Discher, D. E.; Janmey, P.; Wang, Y. L. *Science* **2005**, *310*, 1139-1143.
- (6) Swift, J.; Ivanovska, I. L.; Buxboim, A.; Harada, T.; Dingal, P. C.; Pinter, J.; Pajerowski, J. D.; Spinler, K. R.; Shin, J. W.; Tewari, M.; Rehfeldt, F.; Speicher, D. W.; Discher, D. E. *Science* **2013**, *341*, 1240104.
- (7) Khetan, S.; Guvendiren, M.; Legant, W. R.; Cohen, D. M.; Chen, C. S.; Burdick, J. A. *Nat. Mater.* **2013**, *12*, 458-465.
- (8) Rodríguez-Cabello, J. C.; Martín, L.; Alonso, M.; Arias, F. J.; Testera, A. M. *Polymer* **2009**, *50*, 5159-5169.
- (9) Urry, D. W. *Angew. Chem., Int. Ed. Engl.* **1993**, *32*, 819-841.

- 1
2
3
4
5
6
7
8
9
10
11
12
13
14
15
16
17
18
19
20
21
22
23
24
25
26
27
28
29
30
31
32
33
34
35
36
37
38
39
40
41
42
43
44
45
46
47
48
49
50
51
52
53
54
55
56
57
58
59
60
- (10) Tamburro, A. M.; Guantieri, V.; Pandolfo, L.; Scopa, A. *Biopolymers* **1990**, *29*, 855-870.
- (11) Urry, D. W.; Parker, T. M.; Reid, M. C.; Gowda, D. C. *J. Bioact. Compat. Polym.* **1991**, *6*, 263-282.
- (12) Rodriguez-Cabello, J. C.; Martin, L.; Girotti, A.; Garcia-Arevalo, C.; Arias, F. J.; Alonso, M. *Nanomedicine* **2011**, *6*, 111-122.
- (13) Rodriguez-Cabello, J. C.; Pierna, M.; Fernandez-Colino, A.; Garcia-Arevalo, C.; Arias, F. J. *Adv. Biochem. Eng./Biotechnol.* **2010**, *125*, 145-179.
- (14) Martin, L.; Arias, F. J.; Alonso, M.; Garcia-Arevalo, C.; Rodriguez-Cabello, J. C. *Soft Matter* **2010**, *6*, 1121-1124.
- (15) Betre, H.; Liu, W.; Zalutsky, M. R.; Chilkoti, A.; Kraus, V. B.; Setton, L. A. *J. Controlled Release* **2006**, *115*, 175-182.
- (16) Liu, W.; MacKay, J. A.; Dreher, M. R.; Chen, M.; McDaniel, J. R.; Simnick, A. J.; Callahan, D. J.; Zalutsky, M. R.; Chilkoti, A. *J. Control Release* **2010**, *144*, 2-9.
- (17) Betre, H.; Setton, L. A.; Meyer, D. E.; Chilkoti, A. *Biomacromolecules* **2002**, *3*, 910-916.
- (18) Betre, H.; Ong, S. R.; Guilak, F.; Chilkoti, A.; Fermor, B.; Setton, L. A. *Biomaterials* **2006**, *27*, 91-99.
- (19) Quynh P. Pham, U. S., Dr. Antonios G. Mikos *Tissue Eng.* **2006**, *12*, 1197-1211.
- (20) Zhang, S. *Nat. Biotech.* **2003**, *21*, 1171-1178.
- (21) Altunbas, A.; Pochan, D. J. In *Peptide-Based Materials.*; Deming, T., Ed.; Springer Berlin Heidelberg: Los Angeles, 2011; p 174.
- (22) Takahashi, Y.; Gehoh, M.; Yuzuriha, K. *Int. J. Biol. Macromol.* **1999**, *24*, 127-138.
- (23) Asakura, T.; Yao, J.; Yamane, T.; Umemura, K.; Ulrich, A. S. *J. Am. Chem. Soc.* **2002**, *124*, 8794-8795.
- (24) Hardy, J. G.; Römer, L. M.; Scheibel, T. R. *Polymer* **2008**, *49*, 4309-4327.

- 1
2
3
4
5
6
7
8
9
10
11
12
13
14
15
16
17
18
19
20
21
22
23
24
25
26
27
28
29
30
31
32
33
34
35
36
37
38
39
40
41
42
43
44
45
46
47
48
49
50
51
52
53
54
55
56
57
58
59
60
- (25) Altman, G. H.; Diaz, F.; Jakuba, C.; Calabro, T.; Horan, R. L.; Chen, J. S.; Lu, H.; Richmond, J.; Kaplan, D. L. *Biomaterials* **2003**, *24*, 401-416.
- (26) Cappello, J.; Crissman, J.; Dorman, M.; Mikolajczak, M.; Textor, G.; Marquet, M.; Ferrari, F. *Biotechnol. Prog.* **1990**, *6*, 198-202.
- (27) Dinerman, A. A.; Cappello, J.; Ghandehari, H.; Hoag, S. W. *Biomaterials* **2002**, *23*, 4203-4210.
- (28) Xia, X. X.; Xu, Q.; Hu, X.; Qin, G.; Kaplan, D. L. *Biomacromolecules* **2011**, *12*, 3844-3850.
- (29) Nagarsekar, A.; Crissman, J.; Crissman, M.; Ferrari, F.; Cappello, J.; Ghandehari, H. *J. Biomed. Mater. Res.* **2002**, *62*, 195-203.
- (30) Nagarsekar, A.; Crissman, J.; Crissman, M.; Ferrari, F.; Cappello, J.; Ghandehari, H. *Biomacromolecules* **2003**, *4*, 602-607.
- (31) Haider, M.; Leung, V.; Ferrari, F.; Crissman, J.; Powell, J.; Cappello, J.; Ghandehari, H. *Mol. Pharmaceutics* **2005**, *2*, 139-150.
- (32) Landau, L. D.; Lifshitz, E. M. In *Theory of Elasticity*; 3rd ed.; Kosevitch, A. M., Pitaevskii, L. P., Eds.; Pergamon Press: 1984; p 195.
- (33) Leach, J. B.; Wolinsky, J. B.; Stone, P. J.; Wong, J. Y. *Acta Biomater.* **2005**, *1*, 155-164.
- (34) Girotti, A.; Fernandez-Colino, A.; Lopez, I. M.; Rodriguez-Cabello, J. C.; Arias, F. J. *Biotechnol. J.* **2011**, *6*, 1174-1186.
- (35) Rodriguez-Cabello, J. C.; Girotti, A.; Ribeiro, A.; Arias, F. J. In *Nanotechnology in Regenerative Medicine*; Navarro, M., Planell, J. A., Eds.; Humana Press: 2012; p 319.
- (36) Meyer, D. E.; Chilkoti, A. In *Protein Interactions E Golemis, Ed. Cold Spring Harbor Laboratory Press*; 2nd ed.; Golemis, E., Adams, P. D., Eds.; Cold Spring Harbor Laboratory Press: 2002; p 938.

- 1
2
3
4
5
6
7
8
9
10
11
12
13
14
15
16
17
18
19
20
21
22
23
24
25
26
27
28
29
30
31
32
33
34
35
36
37
38
39
40
41
42
43
44
45
46
47
48
49
50
51
52
53
54
55
56
57
58
59
60
- (37) Megeed, Z.; Cappello, J.; Ghandehari, H. *Adv Drug Deliv Rev* **2002**, *54*, 1075-1091.
- (38) Machado, R.; Azevedo-Silva, J.; Correia, C.; Collins, T.; Arias, F. J.; Rodriguez-Cabello, J. C.; Casal, M. *AMB Express* **2013**, *3*, 1-15.
- (39) Meyer, D. E.; Chilkoti, A. *Nat. Biotechnol.* **1999**, *17*, 1112-1115.
- (40) Meyer, E.; Chilkoti, A. In *Protein-Protein Interactions: A Molecular Cloning Manual*; 2nd ed.; Golemis, E., Adams, P. D., Eds.; Cold Spring Harbor Laboratory Press: 2002; p 938.
- (41) Urry, D. W.; Gowda, D. C.; Parker, T. M.; Luan, C. H.; Reid, M. C.; Harris, C. M.; Pattanaik, A.; Harris, R. D. *Biopolymers* **1992**, *32*, 1243-1250.
- (42) Nystroem, B.; Walderhaug, H.; Hansen, F. K.; Lindman, B. *Langmuir* **1995**, *11*, 750-757.
- (43) Tung, C.-Y. M.; Dynes, P. J. *J. Appl. Polym. Sci.* **1982**, *27*, 569-574.
- (44) Winter, H. H.; Chambon, F. *J. Rheol.* **1986**, *30*, 367-382.
- (45) Anseth, K. S.; Bowman, C. N.; Brannon-Peppas, L. *Biomaterials* **1996**, *17*, 1647-1657.
- (46) Hu, X.; Kaplan, D.; Cebe, P. *Macromolecules* **2008**, *41*, 3939-3948.
- (47) Hu, X.; Kaplan, D.; Cebe, P. *Macromolecules* **2006**, *39*, 6161-6170.
- (48) Hu, X.; Wang, X.; Rnjak, J.; Weiss, A. S.; Kaplan, D. L. *Biomaterials* **2010**, *31*, 8121-8131.
- (49) Kong, J.; Yu, S. *Acta Biochim. Biophys. Sin.* **2007**, *39*, 549-559.
- (50) Lu, Q.; Hu, X.; Wang, X.; Kluge, J. A.; Lu, S.; Cebe, P.; Kaplan, D. L. *Acta Biomater.* **2010**, *6*, 1380-1387.
- (51) Chen, X.; Cai, H.; Ling, S.; Shao, Z.; Huang, Y. *Appl. Spectrosc.* **2012**, *66*, 696-699.
- (52) Martín, L.; Castro, E.; Ribeiro, A.; Alonso, M.; Rodríguez-Cabello, J. C. *Biomacromolecules* **2012**, *13*, 293-298.
- (53) Pinedo-Martín, G.; Castro, E.; Martín, L.; Alonso, M.; Rodríguez-Cabello, J. C. *Langmuir* **2014**, *30*, 3432-3440.

1 (54) Dreher, M. R.; Simnick, A. J.; Fischer, K.; Smith, R. J.; Patel, A.; Schmidt, M.; Chilkoti,
2
3 A. J. *Am. Chem. Soc.* **2007**, *130*, 687-694.

4 (55) Machado, R.; Bessa, P. C.; Reis, R. L.; Rodriguez-Cabello, J. C.; Casal, M. In
5
6
7 *Nanoparticles in Biology and Medicine*; Soloviev, M., Ed.; Humana Press: 2012; p 555.

8 (56) Bessa, P. C.; Machado, R.; Nürnberger, S.; Dopler, D.; Banerjee, A.; Cunha, A. M.;
9
10 Rodríguez-Cabello, J. C.; Redl, H.; van Griensven, M.; Reis, R. L.; Casal, M. *J. Controlled Release*
11
12
13 **2010**, *142*, 312-318.

14 (57) Golinska, M. D.; Pham, T. T. H.; Wertén, M. W. T.; de Wolf, F. A.; Cohen Stuart, M. A.;
15
16
17 van der Gucht, J. *Biomacromolecules* **2013**, *14*, 48-55.

18 (58) Hwang, W.; Kim, B. H.; Dandu, R.; Cappello, J.; Ghandehari, H.; Seog, J. *Langmuir*
19
20
21
22 **2009**, *25*, 12682-12686.

23 (59) Fändrich, M. *Cell. Mol. Life Sci.* **2007**, *64*, 2066-2078.
24
25
26
27
28
29
30
31
32
33
34
35
36
37
38
39
40
41
42
43
44
45
46
47
48
49
50
51
52
53
54
55
56
57
58
59
60

TOC

(EIS)x2 hydrogel